Energy & Environmental Science

Accepted Manuscript

ROYAL SOCIETY OF CHEMISTRY

www.rsc.org/ees

Energy & Environmental Science RSCPublishing

ARTICLE

Renewable hydrogen generation from a dual-circuit redox flow battery

Cite this: DOI: 10.1039/x0xx00000x

Véronique Amstutz,[a] Kathryn E. Toghill,[a] Francis Powlesland,[a] Heron Vrubel,[b] Christos Comninellis,[a] Xile Hu[b] and Hubert H. Girault[a]

Received 00th January 2014,
Accepted 00th January 2014

DOI: 10.1039/x0xx00000x

www.rsc.org/

Redox flow batteries (RFBs) are particularly well suited for storing the intermittent excess supply of renewable electricity; so-called "junk" electricity. Conventional RFBs are charged and discharged electrochemically, with electricity stored as chemical energy in the electrolytes. In the RFB system reported here, the electrolytes are conventionally charged but are then chemically discharged over catalytic beds in separate external circuits. The catalytic reaction of particular interest generates hydrogen gas as secondary energy storage. For demonstration, indirect water electrolysis was performed generating hydrogen and oxygen in separate catalytic reactions. The electrolyte containing V(II) was chemically discharged through proton reduction to hydrogen on a molybdenum carbide catalyst, whereas the electrolyte comprising Ce(IV) was similarly discharged in the oxidation of water to oxygen on a ruthenium dioxide catalyst. This approach is designed to complement electrochemical energy storage and may circumvent the low energy density of RFBs especially as hydrogen can be produced continuously whilst the RFB is charging.

Introduction

With the rapid development of wind and photovoltaic energy technologies in Europe and other parts of the globe, storing an excess supply of electricity is becoming an increasingly prominent issue. Due to their discontinuous and unpredictable nature, they cannot be used on the large-scale to feed the distribution grid alone, requiring mediating platforms to store the energy and release it as needed. Large-scale energy storage systems such as hydroelectric power stations are most often used, but they are geographically restricted. Compressed air (CAES) and liquid air are other promising strategies in addressing the challenge of large scale energy storage[1, 2], though round-trip efficiency can be at best 50%[1, 3]. Alternatively, electrochemical and hydrogen energy storage may provide a medium-to-large scale means of regulating the grid.

Electrochemical energy storage, i.e. batteries and accumulators are efficient and scalable means of storing energy presently[4]. Although effective, simple and well understood, battery technology has been predominantly applied to small portable systems and somewhat larger applications in transportation. Scaling-up the power of these conventional batteries is not convenient, and presently only Li-ion and sodium-sulfur batteries are viable means of attaining high energy density batteries. Yet, large-scale energy storage and distribution structures need not be portable, thus with respect to static electrochemical systems, redox flow batteries (RFBs) are especially well designed for renewable energy storage[5].

Energy storage using RFBs has long been studied[6], with two types of flow battery having been successfully commercialized to-date: the zinc-bromine[7] and all-vanadium RFBs[8]. All-vanadium RFBs, using V(III)/V(II) and V(V)/V(IV) redox couples were proposed by Skyllas-Kazacos *et al.* in 1986[9], and are now widely tested globally for the storage of renewable energy. A number of countries are integrating MW-scale RFB systems into the power grid, including the USA, Japan, Australia and Germany[10]. Thus, as stand-alone energy storage systems, RFBs are a commercially available and established technology.

The advantages of using RFBs as large-scale energy storage systems are numerous. They are very flexible as storage capacity and output power are independent: capacity scales with the concentration and redox species and the volume of electrolyte, whereas stack configuration and the number of cells control the output power. RFBs are also highly responsive with millisecond response time to load or charge, have a long lifetime of over 10 years of continuous charge/discharge cycling, and they are not affected by micro-cycles, i.e. non-complete charge and discharge cycles[10, 11]. Furthermore, they are comparatively low-cost with respect to installation and maintenance, comprise relatively abundant and environmentally considerate materials and are emission free. The main drawbacks with RFBs are their relatively low energy density leading to high investment costs to achieve medium-to-large scale energy storage. Although the electrolyte volume can be increased, it remains that once the electrolytes are charged, the battery can no longer store surplus energy until the electrolytes have been discharged to some extent through a load.

Hydrogen has long been considered a means of storing renewable energy. Theoretically hydrogen is an excellent energy carrier[12], but to reap its benefits and transition smoothly into a functioning hydrogen economy, it must be produced, distributed and consumed efficiently and at low cost. Furthermore, it must be generated via clean and sustainable means, unlike the classical reforming of natural gas or coal. Converting renewable power to hydrogen gas is possible using centralised large-scale electrolysers, in which electrical energy is converted into chemical energy (hydrogen bond) by water electrolysis. Two major types of electrolyser are the alkaline and the proton-exchange-membrane (PEM) electrolysers.

Alkaline electrolysers represent an established and durable system for producing H_2 in very large quantities, yet they are not ideally suited to intermittent electrolysis due to degradation of the nickel electrodes[13]. Furthermore the possibility of H_2 and O_2 recombination within the stack[14], and the formation of bubbles at high current densities, leading to an inhomogeneous current distribution at the electrode surface are prompting alternative technologies to be sought[15]. The efficiency of such systems is also mediocre, typically 50-60% for low temperature alkaline electrolysers at 100-300 A cm^{-2} and their durability is limited due to the caustic media employed[15]. PEM electrolysers are a much newer technology but are rapidly growing in interest and in size, with the conventionally small systems now being scaled-up to large, static electrolysers[14]. Presently, high installation and operating costs, predominantly due to the precious metal catalysts in the stack, prevent PEM electro-generated hydrogen from being a viable economic commodity and wide spread energy carrier.

Separating water splitting reactions from the electrochemical processes will provide a means to avoid H_2 and O_2 recombination and electrode degradation. The temporal and spatial decoupling of the oxygen and hydrogen evolution reactions using polyoxometalate mediator were recently reported by Symes and Cronin[16]. In the system presented herein, the catalysed water splitting reactions occur in separate circuits, in parallel with the RFB central circuit. Indirect water electrolysis is achieved over two catalytic beds, using the charged redox species of a conventional V-Ce RFB as electron donor and acceptor for the hydrogen or oxygen evolution reactions. The proposed dual circuit system (Figure 1) has the advantage of providing a secondary platform to store surplus energy beyond the capacity of the charged electrolytes, in the form of hydrogen. It is therefore a complementary technology allowing renewable electricity that would otherwise be lost when the RFB is as full capacity. Furthermore, the catalytic reactions occur independently of the electrode processes providing the opportunity to use low-cost, non-precious catalysts to obtain the hydrogen.

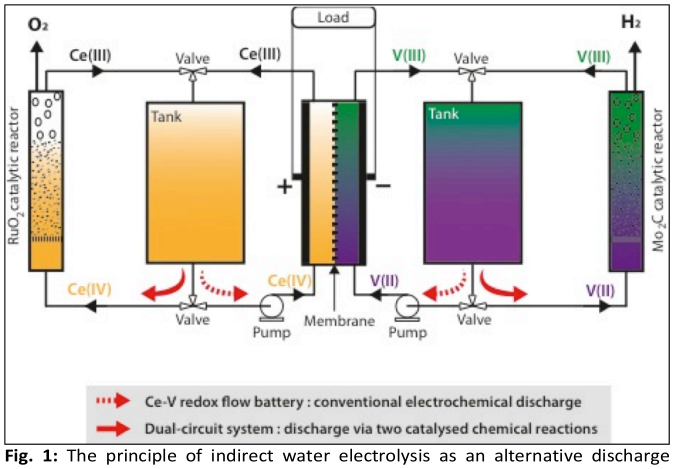

Fig. 1: The principle of indirect water electrolysis as an alternative discharge process for a V-Ce RFB. Once in the charged state (V(II) and Ce(IV)) both electrolytes may be directed in an external catalytic bed to be chemically regenerated, and then return to the redox flow battery. The catalysed chemical reactions taking place in the catalytic beds allow the generation of hydrogen from the catholyte (V(II)) and oxygen from the anolyte(Ce(IV)).

Results and discussion

V – Ce redox flow battery.

All-vanadium RFBs have undergone extensive studies regarding thermodynamics, kinetics, cell design and stability[10, 11, 17]. The cathodic redox couple, V(III)/V(II), has a standard potential of –0.26 V *vs.* SHE. It is stable in strongly acidic conditions, but is hydrolysed and precipitates at pH values higher than 2.5[18]. The high solubility of V(III) and V(II) in acidic conditions allows for concentrations of up to 5 M in sulfuric acid[19]. The reduction and oxidation potentials for the V(III)/V(II) redox couple were determined on polymer rod graphite electrodes via cyclic voltammetry of V(III) in sulfuric acid (Figure S1, ESI). The cyclic voltammogram corresponds well to literature in which it has been reported that this redox couple has reasonably fast kinetics on carbon or graphite felt electrodes in various acidic conditions[20-23]. On the graphite polymer rod in particular, the vanadium gave quite reversible behaviour, with a peak separation of 67 mV and an $E_{1/2}$= –0.3 V *vs.* SHE at a scan rate of 20 mV/s. The graphite felt cyclic voltammograms were less defined, due to saturation of the porous material, nonetheless, reduction and oxidation peaks were evident in the region of –0.25 V *vs.* SHE (not shown).

The redox couple Ce(IV)/Ce(III) is largely used for redox titration, and the Ce(IV) species as an oxidative reagent in organic chemistry[24]. In the field of energy storage it has been employed in zinc-cerium RFBs[25, 26], but relatively few studies have regarded V–Ce RFBs[25, 27-30]. The cerium standard potential depends on the nature of the cerium complex, i.e. on its coordination shell, which in turn is related to the nature of the acid and the initial cerium salt. It ranges from 1.28 V in 1 M hydrochloric acid to 1.70 V in 1 M perchloric acid[24]. Methanesulfonic acid (MSA) may also be used as a supporting electrolyte, either alone, or mixed with sulfuric or nitric acid. MSA is of interest due to its properties of being a "green" solvent and incurring reduced corrosion of electrode materials. It can also significantly increase the solubility of both Ce(III) and Ce(IV) ions[25, 29]. The Ce(III)/Ce(IV) oxidation and reduction potentials in MSA were reported to be 1.65 V and 1.05 V *vs.* SHE on a platinum electrode, displaying quasi-reversible behaviour[25]. In a 1:1 mixed MSA/H_2SO_4 solution however, the Ce(III)/(IV) couple becomes considerably more reversible with a peak potential difference of just 103 mV reported by Xie *et al.*[29]. Finally, sulfamic acid has also been studied in which quasi-reversible behaviour was observed and the redox potential was 1.52 V *vs.* SHE[30].

Sulfuric acid, nitric acid and MSA were studied as the common acidic media in the V–Ce RFB due to the variation in redox potentials expected. The addition of MSA to both nitric and sulfuric acids was also evaluated. Cyclic voltammetry was conducted on platinum and graphite electrodes, with a pre-treatment procedure applied to the platinum as outlined in previous literature[31]. A comparison between cyclic

voltammograms of Ce(IV) in 1:1 H_2SO_4:MSA and 1:1 HNO_3:MSA acid mixtures on graphite polymer rod electrode is shown in Figure S2 (ESI). Both media gave quasi-reversible behaviour, and half-wave potentials of *ca.* 1.48 V *vs.* SHE for the H_2SO_4 mixture, and 1.61 V *vs.* SHE for the HNO_3 mixture were obtained. Although nitric acid gave a more reversible voltammetric performance, its potential use in the RFB is limited due to the cross contamination of nitrate anions through the membrane resulting in the formation of lower nitrous oxides and the self-discharge of vanadium species. Furthermore, nitric acid requires a much more oxidative potential at the anode and also corrodes the anode electrode at an appreciable rate.

The anodic and cathodic redox couples were selected based on their ability to oxidize water and reduce protons in acidic conditions. The redox potential of the V(III)/V(II) couple renders the V(II) species highly suited to electron donation in the hydrogen evolution reaction (HER), yet to our knowledge, the use of V(II) in this capacity has only been studied briefly in the early 1980s[32, 33]. In these publications, Parmon *et al.* used the V(II) as a reductant alongside a rhodium polyamine complex as HER catalyst. In the same vein Ce(IV) has frequently been used for testing water oxidation catalysts in low pH.[34-36] Note that although both V(II) and Ce(IV) are thermodynamically capable of driving water splitting reactions, they are kinetically incapable, and only proceed in the presence of a catalyst.

In sulfuric acid, the V-Ce RFB thermodynamic cell potential is 1.7 V, which is much higher than the all-vanadium battery (1.26 V). However, only a few studies on the V-Ce RFB have been reported[25, 27-30], and opinion of the system is somewhat divided. In order to test the feasibility of this battery for the present application, we designed and built a single-celled V-Ce RFB. Pre-treated graphite felt electrodes were used, with 100 mM of Ce(III) sulfate and 100 mM V(IV) sulfate (converted to V(III)) in 1M H_2SO_4, attaining the mean charging and discharging cell potentials of 2.5 V and 0.7 V (at 60 $mA \cdot cm^{-2}$). The charging and discharging curves shown in Figure S3 (ESI) were measured under galvanostatic conditions and controlled by a galvanostat-potentiostat. The charging proceeded over 1h and 10 min, at 60 $mA \cdot cm^{-2}$, and the discharging process was similar in length. Charging and discharging coulombic efficiencies were very high at 94% and 96%. Neither oxygen or hydrogen evolution was observed up to current densities of 80 $mA \cdot cm^{-2}$, except at the very end of the galvanostatic charging and discharging processes. The difference between charging and discharging cell potentials is due to a combination of ohmic drop and sluggish kinetics. The most dominant sources of internal resistance stem from the central Nafion membrane and the graphite felt electrodes imparting some resistance due to poor conductivity. The electrodes were improved to some extent by heat treatment, but were not thoroughly optimised. Furthermore, the quasi reversibility of both redox couples employed also decreases the voltage efficiency of the battery, especially on the Ce(IV)/Ce(III) side (Figure S2, ESI).

Multi-cyclic experiments indicated that the anode slightly degraded, as small black particles were visible in the cerium anolyte at high cell potential. Furthermore vanadium cations were found to be crossing the Nafion membrane, evident in the blue tinge of the Ce(III) solutions that were initially transparent. However, this only clearly occurred when the V-Ce RFB was under deep discharge and charge conditions, *i.e.* when the mediators were almost or totally converted.

A number of impeding limitations stem from the use of the cerium mediator in the system, specifically the degradation of the carbon-based electrode due to the high oxidative power of Ce(IV) and its requirement for a high anodic potential, the low solubility of Ce(III) and Ce(IV) compounds, and the difficult chemistry of Ce(III) and Ce(IV) ions, which form complex precipitates, and are very sensitive to the nature and pH of the solution. A number of these problems may be avoided however by using an alternative anode to carbon (*e.g.* boron doped diamond or titania), introducing additives such as MSA to improve solubility, and gaining further understanding of the cerium chemistry with respect to the acidic medium. Optimisation of the V-Ce RFB was not the main goal of this project and has been undertaken by other researchers[25, 27, 37]. Nonetheless, to demonstrate indirect water splitting the V-Ce RFB is highly suited, as in the present system, the intended discharge is not electrochemical, but chemical.

Indirect water electrolysis.

Conventionally, RFBs retain their electrically charged redox states until connecting to an electrical load to discharge. Alternatively, both initial redox species (V(III) and Ce(III)) may be regenerated through two separate catalysed chemical reactions, generating H_2 and O_2 in the process. In the present system, the electrolyte containing Ce(IV) is passed through a secondary circuit, consisting of a catalytic bed composed of RuO_2 or IrO_2 nanoparticles (generation of O_2, equation (1)), whereas the electrolyte containing V(II) is flowed through a second external catalytic bed, containing Mo_2C catalytic particles (generation of H_2, equation (2)), as depicted in Figure 1. Both electrolytes then return to the central V-Ce RFB and the charging process is repeated. This novel system has been patented[38].

A particular advantage to chemically discharging the V-Ce RFB electrolytes is that suitable design of the catalytic bed could allow the discharge to proceed considerably faster compared to conventional electrochemical discharge. This means that during peak energy production the chemical discharge allows more energy storage per unit time, therefore this system has a higher energy density than a conventional RFB. Chemical discharge could even take place at the same time as electrochemical charging if the configuration of the system is modified. The process of indirect water electrolysis is thus an alternative way of discharging the V-Ce RFB, providing a higher energy storage capacity than conventional RFBs in the form of hydrogen without considerably higher initial investment costs. The proton balance is respected if we consider two cycles and the OER and HER equations (1) and (2) below, where A is electron acceptor and D electron donor.

$$2H_2O + 4A^+ \xrightarrow{\text{Catalyst I}} O_2 + 4H^+ + 4A \quad (1)$$

$$4H^+ + 4D^- \xrightarrow{\text{Catalyst II}} 2H_2 + 2D \quad (2)$$

Although proton consumption and production will occur in the catalytic chambers, it is relative to the concentration of charged redox species. As the proton concentration is an order of magnitude higher in our lab-scale system the pH of the system will remain strongly acidic. The protons produced during water oxidation in the anolyte during the first cycle return to the V-Ce RFB, where they can pass through the proton-exchange membrane during the charging process of the second cycle and finally be reduced at the Mo_2C catalytic bed. Thus the battery

need only be supplemented with water in stoichiometric quantities to the H_2 and O_2 generated.
Catalytic chambers were designed in glass tubes containing microporous fritted glass to filter the electrolyte solutions and prevent the catalytic particles from entering the main battery circuit. The electrolyte descended upon a catalytic bed following diversion from the RFB using a simple 3-way valve, returning to the electrolyte reservoir following chemical discharge. Two stills show hydrogen evolution and oxygen evolution in Figure 2. In practice the produced hydrogen and oxygen gases may be retained in storage tanks leading from the catalytic chambers. Though atmospheric pressure and room temperature conditions were used, a heat exchanger and a compressor could allow higher-pressure hydrogen to be stored.

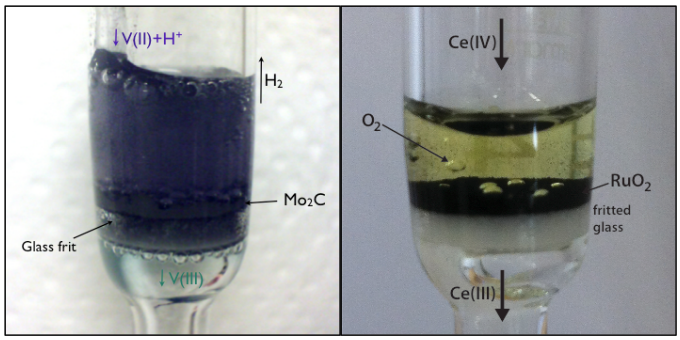

Fig. 2: Photographs of the catalytic reactions. Left: hydrogen evolution from an acidic V(II) solution on a Mo_2C catalytic bed. Right: water oxidation to oxygen from an acidic Ce(IV) solution on a RuO_2 catalytic bed. Hydrogen and oxygen bubbles are clearly visible.

The overall energy efficiency of this system, *i.e.* the ratio between the energy "contained" in the produced hydrogen and the electrical energy required to fully charge the V-Ce RFB is ca. 50 %, considering a 60 $mA \cdot cm^{-2}$ charging current density, 2 cm^2 electrodes, a 70 min charge time, the lower heating value for hydrogen (241 $kJ \cdot mol^{-1}$) and assuming a HER yield of 100% (see ESI for a detailed calculation). The maximum thermodynamic efficiency possible from this reaction is 73%, with the 23% loss observed in the experimental lab-scale reaction is due to the battery charging performance. The difference between theoretical and experimental values may be attributed to the low voltage efficiency observed during the charge of the battery. Further optimisation of the V–Ce RFB is required in order to improve the overall efficiency of the system, particularly those of the electrodes and membrane. However, assuming the generation of hydrogen would be a means of storing surplus electricity (*i.e.* it would be lost if not stored), the overall efficiency of the system is not the most relevant criteria for future applications.

The hydrogen evolution reaction.

The use of molybdenum-based electrocatalysts for the proton reduction reaction in acidic solutions has been revisited in recent years. Initially MoS_2 was recognised and successfully used in the HER,[39-41] but very recently Mo_2C has shown an even better capability and stability[42-44]. When integrated into an electrode, these materials display an overpotential of 150 mV for hydrogen evolution (at 10 $mA \cdot cm^{-2}$), and relatively long-term stability[43]. In the present system, the catalyst (in the form of micro particles) is used as a heterogeneous catalyst in a fixed bed configuration, and V(II) ions play the role of electron donors. The overall reaction, a redox reaction between V(II) and protons, is given by equation (3).

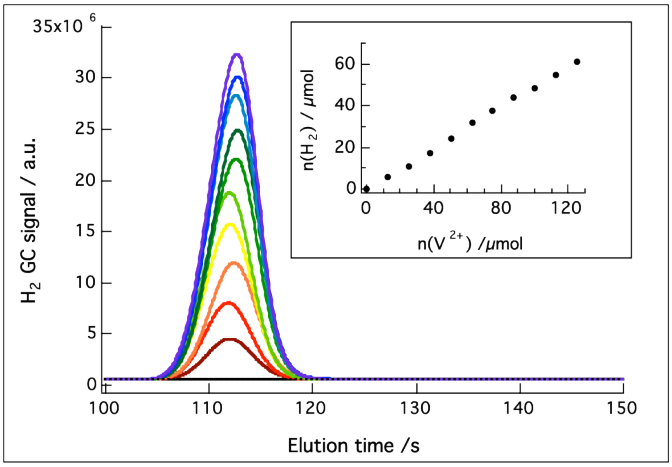

Fig. 3: Hydrogen GC signals for 2 mL solutions containing various concentrations of V(II) (0, 10, 20, 40, 50, 60, 80, 100, 150, and 200mM) in 1 M H_2SO_4 and 1 mg of Mo_2C. The inset shows the amount of hydrogen produced for the corresponding initial amount of V(II) in the solution.

$$2H^+ + 2V^{2+} \xrightarrow{Mo_2C} H_2 + 2V^{3+} \qquad (3)$$

The global parameters of this catalytic hydrogen evolution reaction were determined by means of UV-vis spectroscopy. The solutions of 1 M sulfuric acid and 40 mM V(II) were prepared in the V-Ce RFB. The catalyst (1 ± 0.05 mg) was dispersed in 2 mL of the solution by stirring, and UV-vis spectra of the solution were measured continuously as a function of time between 480 and 1000 nm. In this spectral range the violet electron donor V(II), displays two absorption peaks with maxima at 850 nm and 570 nm, and turns to green V(III) upon oxidation, exhibiting a single absorption peak with a maximum at 600 nm. To monitor the reaction the second V(II) absorption peak (850 nm) was followed due to the overlap of the V(III) and first V(II) peaks (Figure S4, ESI).
The first three minutes of the reaction were considered to determine the reaction order. The rate of reaction (3), v, was found to be first order with respect to the V(II) concentration in 1 M sulfuric acid solutions, and in the presence of 1 mg of Mo_2C. In such conditions, the apparent rate constant k_{app} for this reaction was determined to be $k_{app} = 5.9 \cdot 10^{-3} \pm 0.2 \cdot 10^{-3}\ s^{-1}$. Detailed calculations are given in the ESI. Further measurements showed that the rate of reaction also varied with the amount of catalyst and proton concentration (pH value), indicating that these species are also implicated in the rate-limiting step of the reaction mechanism.
In order to detect possible by-products or side reactions, a batch of samples containing various V(II) concentrations, with an identical amount of dispersed catalyst were tested in septum-sealed glass vials. The reactions were driven to completion by mixing the solutions for at least two hours. The amount of hydrogen contained in the headspace of each glass vial was measured by gas chromatography (GC), and compared to a calibration curve. The reaction yield was 96 ± 4 % as shown in Figure 3, showing no significant side reaction occurred and nearly maximum conversion efficiency was achieved.

The water oxidation reaction.

Water oxidation is a notoriously difficult reaction due to kinetic limitations related to high-energy barriers for the formation of intermediates and transition states[45, 46]. It is especially difficult in acidic conditions, as most studied catalysts operate in neutral or alkaline solutions. Catalysed chemical water oxidation in strongly acidic conditions was therefore studied in detail in order to determine its feasibility and efficiency, using IrO_2 nanoparticles or RuO_2 microparticles as catalyst and Ce(IV) as electron donor.

In 1 M strong acid (H_2SO_4, HNO_3, MSA or acids mixtures) conditions the pH of the solution is 0, therefore the standard potential for water oxidation into oxygen is 1.23 V *vs.* SHE. It was first observed that Ce(IV) sulfate in sulfuric acid, with a standard potential of 1.44 V *vs.* SHE, was not able to oxidise water in presence of supported IrO_2, however with heat pre-treated RuO_2 microparticles the reaction did proceed. This indicated that the overpotential imparted by the catalysts was crucial. The difference in the catalytic potential of different water oxidation catalysts is recognised in the literature, with an OER catalytic potential of 1.44 V (the same as Ce(IV)/Ce(III) in 1 M H_2SO_4) attributed to IrO_2 and a catalytic potential of 1.36 V[47-49] to RuO_2.

As previously mentioned, the Ce(IV)/Ce(III) standard potential depends on the ligands attached to the cerium centre, and was reported to vary between 1.28 V and about 1.7 V *vs*. SHE[24]. An investigation of various acids, mixtures of acids, and cerium salts, in terms of electrochemical reversibility on graphite electrodes and efficiency as electron acceptor in the OER, was conducted. Pre-studies showed that in nitric acid, MSA, and mixtures of both, the IrO_2 catalysed OER (equation 4) was possible using cerium ammonium nitrate (CAN) as the initial salt. More details are given in the ESI (Figure S5).

$$4Ce^{4+} + 2H_2O \xrightarrow{RuO_2 \text{ or } IrO_2/SiO_2} 4Ce^{3+} + 4H^+ + O_2 \qquad (4)$$

The kinetics of the OER using Ce(IV) sulfate generated in 1 M H_2SO_4 in the V-Ce RFB were studied using the pre-treated RuO2 catalyst. RuO_2 is the most widely studied water oxidation catalyst. The catalyst used here was commercial, hydrated RuO_2 that was heated in air at 150 °C overnight, as per the procedure outlined by Mills and Russell[50]. Anhydrous and as-bought hydrous RuO_2 were also studied, and were entirely inactive towards water oxidation. The pre-treated material was highly active however, and seemingly fully converted the Ce(IV) to Ce(III).

In Figure S6 (ESI), the generation of oxygen, and the corresponding consumption of Ce(IV) as a function of the amount of catalyst added to the shake flask is shown. Based on three identical measurements (0.5 mg RuO_2 + 0 to 50 mM Ce(IV) sulfate in 1 M H_2SO_4, high mixing rate, under N_2 atmosphere), the reaction order in the first three minutes for reaction (4) was observed to be unity with respect to Ce(IV) concentration. An apparent rate constant of $k_{app} = 3.08 \cdot 10^{-4} \pm 0.34 \cdot 10^{-4}$ $s^{-1}$was found for the same measurements. Detailed calculations are given in the ESI. The yield of the reaction was measured by varying the concentration of Ce(IV), keeping all the other experimental conditions constant, and by driving the reaction to completion. The amount of oxygen produced was then measured by GC and compared to the amount of Ce(IV) initially present in the solution (Figure 4). The mean conversion over 10 samples was 78 ± 8 %, which indicates the presence of side reactions. Mills and Russell[50] suggested that RuO_2, when hydrated, is corroded by the Ce(IV) cations according to equation (5). Even if the catalyst is expected to be only partially hydrated[50], Ce(IV) ions may have been consumed by this oxidation reaction. This was also supported by the observation that the catalyst was becoming less active with reaction time, and when reused several times.

$$4Ce^{4+} + RuO_2 \cdot xH_2O + 2H_2O \rightarrow 4Ce^{3+} + RuO_2 + xH_2O + 4H^+ \qquad (5)$$

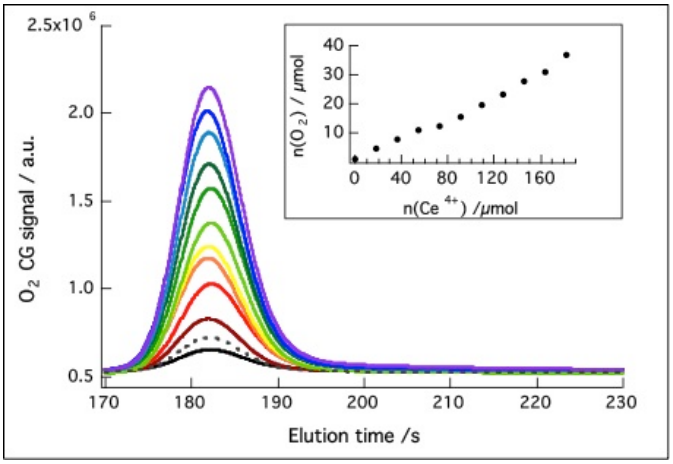

Fig. 4 : Oxygen GC signals for 2 mL solutions of Ce(IV) (0, 10, 20, 30, 40, 50, 60, 70, 80, 90 and 100 mM) in 1M H_2SO_4 and 0.5 mg of hydrated RuO_2. The dashed line is for 100 mM of Ce(IV), without catalyst. Reaction time was at least 2 hours. The inset displays the amount of oxygen which was produced for the corresponding initial amount of Ce(IV) in the solution.

Thermodynamics *vs.* kinetics.

The key concept central to this paper is the interplay of theoretical thermodynamic water electrolysis and the kinetically feasible process. As illustrated in Figure 5 there is a large difference between the thermodynamic potentials for water electrolysis (HER 0V, OER 1.23 V *vs.* SHE) and the generally observed potentials *i.e.* the kinetic overpotentials. Generally, by employing catalysts these overpotentials can be decreased and water electrolysis may occur at potentials closer to the theoretical, however, for water oxidation in particular, the intrinsic kinetic barriers owing to the multi proton and multi electron reaction remain. Electrochemical water oxidation is rarely achieved with less than 200 mV overpotential, with commercial electrolysers usually operating at a cell potential of about 2 V.

In the system proposed here the RFB redox reactions occur at potentials in between the thermodynamic lower limit and kinetic upper limit. When little overpotential is required to drive the reaction, as is the case for the V(III)/(II) reaction, then a solution of electron donor may be readily produced with high coulombic efficiency. In a chemical reaction in the presence of a catalyst the donor can effectively donate those electrons to produce hydrogen and V(III), at a rate that far exceeds electrochemical transfer and with stoichiometric control and very high efficiency. Although cerium oxidation is less kinetically favourable, depending greatly on the acid medium, it too can be converted at a potential intermediate of the thermodynamic and kinetic limits. Optimisation and careful selection of the RFB electrolytes may lead to electrolytic processes that are more favourable than direct electrolysis at an

electrode.

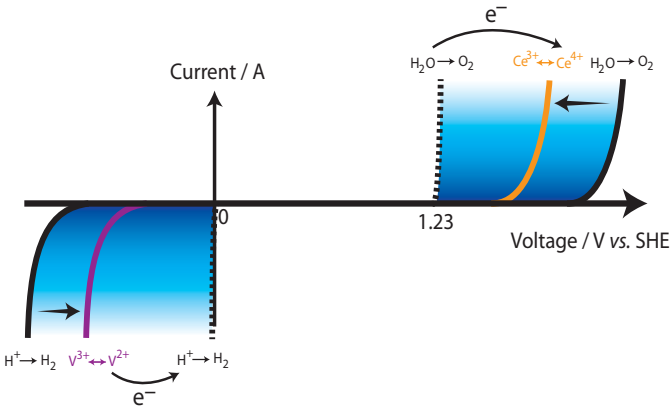

Fig. 5: Principle of indirect water electrolysis. On this scheme, the thermodynamic reduction potential for both reactions of water electrolysis, hydrogen evolution and oxygen evolution (dashed lines), are compared to the actual electrode potential applied to observe these reactions on graphite electrodes (black lines) and the intermediate redox potentials of suitable redox mediators *e.g.* V(III)/(II) and Ce(IV)/(III).

The focus of the dual-circuit RFB is the generation of hydrogen at the cathodic catalytic bed and not the process of oxygen evolution. As a proof of concept indirect water electrolysis presented here completes the modified RFB circuit, allowing for the chemical discharge of both charged electrolytes. However, the potential for numerous alternative anolyte discharge processes is available, including chlorine evolution, the chemical oxidation of organic pollutants, hydrazine oxidation (to N_2 and protons) and sulfur dioxide oxidation to sulfuric acid. Furthermore, the system is not limited to using cerium in the anolyte, as an all-vanadium RFB that can be chemically discharged in some similar manner could also be considered. The concept here is indirect electrolysis, in which hydrogen is evolved effectively and efficiently from a charged vanadium catholyte, and oxygen from the charged cerium anolyte.

Conclusions

An alternative indirect water electrolysis process, based on a dual-circuit V-Ce RFB has been presented. Electrical energy is used to electrochemically reduce and oxidise vanadium and cerium species respectively during the conventional charging of the RFB. In the charged state, the positive redox mediator is used as an electron acceptor in catalysed water oxidation, whereas the negative redox mediator is used as an electron donor in catalysed proton reduction. This chemical discharge takes place in two separate catalytic beds forming a secondary circuit that is appended to the central V-Ce RFB. The system is thus capable of storing electrical energy in the form of charged redox species, or in the hydrogen-hydrogen bond, the latter reproducing the discharged species for reuse in the battery during periods of peak electricity production.

For an all sulfuric acid battery, the coulombic charging efficiency of the battery is 94 % (at 60 $mA{\cdot}cm^{-2}$). Hydrogen was generated from V(II) using an abundant and low cost Mo_2C catalyst and achieved a production yield of 96 ± 4 %. Water oxidation was achieved over IrO_2 and RuO_2 nanoparticles from positive electrolytes comprising Ce(IV) in various acid solutions. A 78 ± 8 % O_2 yield was obtained in 1 M H_2SO_4 and a partially hydrated RuO_2 catalyst.

This system is unique in the field of energy storage, merging two highly pursued technologies: renewable electrochemical energy storage and renewable power-to-gas. The novel technique allows surplus electricity to be stored as hydrogen beyond the limited energy density of the RFB electrolytes, with rapid discharge of the electrolytes also possible to provide an immediate sink for excess electricity. As water oxidation is not of commercial interest, alternative discharge reactions for the anolyte must be investigated. With commercial all-vanadium RFBs the chemical discharge of the positive (V(V)) species may also be envisaged, such as reduction by hydrazine to produce protons and N_2, SO_2 oxidation to produce H_2SO_4, or the oxidation of wastewater pollutants. Further investigations into optimising the anolyte discharge and to further characterise the catalytic reactions are in progress.

Experimental

Redox flow battery.

The anodic solutions prepared were 0.1 M Ce(III) from either the cerium(III) sulfate hydrate (Aldrich) ammonium cerium(III) nitrate (CAN) (ACS 99 %, Acros Organics) in 50 mL of 1 M strong acid (H_2SO_4, HNO_3, methanesulfonic acid, or mixture of acids with a total concentration of 1 M). Similarly, a cathodic solution of 0.1 M vanadium was prepared from $VOSO_4$ in 1 M H_2SO_4. The acid solutions were prepared by diluting concentrated nitric acid (65 %, Fluka), concentrated sulfuric acid (ISO 95-97 %, Merck) or methanesulfonic acid (methanesulfonic acid solution, 70 wt %, Sigma-Aldrich) in Ultrapure water (18.2 MΩ·cm). Solutions were deoxygenated in their RFB storage tanks for at least 20 minutes with nitrogen (N_2 45, Carbagas) before being circulated through the battery at a constant flow rate of 50 $mL{\cdot}min^{-1}$. A continuous flow of nitrogen was maintained in both storage tanks during the charging and discharging processes.

The electrochemical cell was built in-house using custom designed Teflon pieces. A full description and corresponding figure of the system is given in the ESI (Figure S7). In brief, the cell consisted of two Teflon external parts, two 3 mm thick Viton seals, and a pre-treated Nafion® N117 ion-exchange membrane (Ion Power Inc.). Each half-cell contained a boron doped diamond (W260, Adamantec) current collector plate mounted on stainless steel, which was connected to the external electrical circuit on the backside through a steel rod. The electrodes were graphite felt (Sigratherm GFD5 EA, SGL Group) of dimension 0.5 x 0.5 x 4 cm. They were pre-treated by heating in an oven at 400°C for 4 hours in air. A peristaltic pump (Reglo Dig. MS, Ismatec) was used to drive both electrolytes through the Teflon tube circuit. An Autolab (PGSTAT128N, Metrohm Autolab B.V.) was used to measure the galvanostatic charge and discharge of the RFB and two multimeters (UNI-T UT71E, Uni-Trend Technology Limited, China) were used to monitor the discharge when an external resistance was used.

The total concentration of vanadium, respectively cerium was measured by ICP-OES analysis performed with an Optima 2000 spectrometer (Perkin-Elmer). A standard TraceCERT (1 g/L, Aldrich) was used for vanadium calibration, whereas a standard solution of cerium(IV) ammonium nitrate (Aldrich) was prepared from a dried salt (heated at 85°C overnight) and

used for cerium calibration. The concentration of Ce(IV) in the solution was also measured by indirect iodine titration. A known volume of the analysed solution was diluted in 10 mL of a 1M sulfuric acid solution and an excess of potassium iodide (Fluka) was added. The iodine produced was titrated with sodium thiosulfate (anhydrous, 99%, Alfa Aesar), and a small amount of potato starch (Fluka).

Catalytic beds.

The catalytic beds were prepared from glass funnel containing a fritted glass filter (Por. 4, 11 to 16 µm). Catalytic powder was placed on top of the fritted glass, and the charged RFB solution was diverted using a 3-way valve to flow through the catalytic layer and the filter. The flow rate of the electrolytes through the catalytic beds was about 1 $mL \cdot min^{-1}$. Such a low value was required due to the flow resistance exhibited by the fritted glass and the catalytic bed. After the reaction, the flow of discharged solution was redirected to the appropriate storage tank in the RFB.

Catalyst preparation.

Mo_2C (325 mesh, Aldrich) catalyst was used as received for the kinetic measurements. Structural information on the catalyst have been reported elsewhere[43]. The catalytic bed was first treated with a 1 M H_2SO_4 solution, in order to remove the particles small enough to pass through the fritted glass, to prevent any from entering the redox flow battery.
Hydrated RuO_2 (ruthenium(IV) hydrate, Fluka) was pre-treated in accordance to studies by Mills and Russell[50]. A portion of the compound was partially dehydrated in air at 150°C for at least 6 hours. The catalyst was then used directly to form a catalytic bed in a Por. 4 fritted glass tube. The synthesis procedure for IrO_2 nanoparticles immobilised on SiO_2 is detailed in the ESI.

UV-vis measurements.

All UV-vis measurements were conducted inside a glovebox (maximum oxygen content: 3 ppm). Calibration curves for V(II) and V(III) were established between 0 and 100 mM in 1 M sulfuric acid solutions. The kinetics were analysed using a spectrophotometer (CHEM2000 UV-vis, Ocean Optics, Switzerland) placed on a magnetic plate to allow constant agitation of the sample. The blank was always the corresponding acid solution. For the kinetic measurements, the UV-vis spectra as a function of time were recorded automatically with the software OOIBase32 (Version 1.0.3.0, Ocean Optics).

Gas quantification.

A gas chromatograph (AutoSystem, Perkin Elmer) based on an injection loop, a molecular sieve packed column (12' x 1/8'' SS Column, Molecular Sieves 5A 100/80, Perkin Elmer), and a TCD detector were used for the quantification of oxygen and hydrogen. To proceed to the measurement, the headspace of the septum-sealed flask was sampled with a gastight lock-in syringe, and then injected into the injection loop of the gas chromatograph. The obtained data were compared to a calibration curve.
To determine the water oxidation kinetic parameters reactions were conducted using fluorimetric oxygen sensor (NeoFox, FOXY probe, OceanOptics) in 4 mL septum-sealed flasks, under a nitrogen atmosphere. All solutions were deoxygenated and the catalyst powder added to the flask (in the glovebox) before the setup of the flask in the deoxygenated NeoFox compartment. The reactive solution (2 mL) was added through the septum with a syringe and the oxygen detector measured the amount of oxygen in the headspace of the flask as a function of time. Data were recorded automatically every 500 ms.

Acknowledgements

The present project is supported by EOS Holding SA (Switzerland) for LEPA and by the European Research Council for LSCI (starting grant no. 257096). We thank Micheál Scanlon and Jonnathan Hidalgo for their help regarding the IrO_2 catalyst.

Notes and references

[a] *Ecole Polytechnique Fédérale de Lausanne, EPFL-SB-ISIC-LEPA, Station 6, CH-1015 Lausanne, Switzerland.*
[b] *Ecole Polytechnique Fédérale de Lausanne, EPFL-SB-ISIC-LSCI, BCH 3305CH-1015 Lausanne, Switzerland.*

† Electronic Supplementary Information (ESI) available: ESI includes charging and discharging curves, cyclic voltammetry, UV-vis spectra of V(II) and V(III), a picture of the cell, details on the kinetics measurement and calculations. See DOI: 10.1039/b000000x/

1. H. Chen, T. N. Cong, W. Yang, C. Tan, Y. Li and Y. Ding, *Progress in Natural Science*, 2009, 19, 291-312.
2. H. Lund and G. Salgi, *Energy Conversion and Management*, 2009, 50, 1172-1179.
3. H. Ibrahim, A. Ilinca and J. Perron, *Renewable and Sustainable Energy Reviews*, 2008, 12, 1221-1250.
4. B. Dunn, H. Kamath and J. M. Tarascon, *Science*, 2011, 334, 928-935.
5. T. Nguyen and R. F. Savinell, *Electrochem. Soc. Interface*, 2010, 19, 54-56.
6. *US Pat.,* 3,996,064, 1976.
7. *US Pat.,* 4,491,625, 1985.
8. *US Pat.,* 4,786,567, 1988.
9. M. Skyllas-Kazacos, *Journal of the Electrochemical Society*, 1986, 133, 1057.
10. A. Z. Weber, M. M. Mench, J. P. Meyers, P. N. Ross, J. T. Gostick and Q. Liu, *Journal of Applied Electrochemistry*, 2011, 41, 1137-1164.
11. M. Skyllas-Kazacos, M. H. Chakrabarti, S. A. Hajimolana, F. S. Mjalli and M. Saleem, *Journal of the Electrochemical Society*, 2011, 158, R55.
12. A. Midilli, M. Ay, I. Dincer and M. A. Rosen, *Renewable and Sustainable Energy Reviews*, 2005, 9, 255-271.
13. W. Hu, *International Journal of Hydrogen Energy*, 2000, 25, 111-118.
14. M. Carmo, D. L. Fritz, J. Mergel and D. Stolten, *International Journal of Hydrogen Energy*, 2013, 38, 4901-4934.
15. K. Zeng and D. Zhang, *Progress in Energy and Combustion Science*, 2010, 36, 307-326.
16. M. D. Symes and L. Cronin, *Nat Chem*, 2013, 5, 403-409.

17. C. Ponce-de-León, A. Frías-Ferrer, J. González-García, D. A. Szánto and F. C. Walsh, *Journal of Power Sources*, 2006, 160, 716-732.
18. K. Post and R. G. Robins, *Electrochimica Acta*, 1976, 21, 401-405.
19. F. Rahman and M. Skyllas-Kazacos, *Journal of Power Sources*, 1998, 72, 105-110.
20. C. Gao, N. Wang, S. Peng, S. Liu, Y. Lei, X. Liang, S. Zeng and H. Zi, *Electrochimica Acta*, 2013, 88, 193-202.
21. K. J. Kim, Y.-J. Kim, J.-H. Kim and M.-S. Park, *Materials Chemistry and Physics*, 2011, 131, 547-553.
22. X. Li, K. Huang, S. Liu, N. Tan and L. Chen, *Transactions of Nonferrous Metals Society of China*, 2007, 17, 195-199.
23. X. W. Wu, T. Yamamura, S. Ohta, Q. X. Zhang, F. C. Lv, C. M. Liu, K. Shirasaki, I. Satoh, T. Shikama, D. Lu and S. Q. Liu, *Journal of Applied Electrochemistry*, 2011, 41, 1183-1190.
24. K. A. J. Gschneidner, J.-C. G. Bünzli and V. K. Pecharsky, *Handbook on the Physics and Chemistry of Rare Earths*, Elsevier, 2006.
25. P. K. Leung, C. Ponce-de-León, C. T. J. Low and F. C. Walsh, *Electrochimica Acta*, 2011, 56, 2145-2153.
26. G. Nikiforidis, L. Berlouis, D. Hall and D. Hodgson, *Journal of Power Sources*, 2012, 206, 497-503.
27. Y. Liu, X. Xia and H. Liu, *Journal of Power Sources*, 2004, 130, 299-305.
28. X. Xia, H.-T. Liu and Y. Liu, *Journal of the Electrochemical Society*, 2002, 149, A426.
29. Z. Xie, F. Xiong and D. Zhou, *Energy & Fuels*, 2011, 25, 2399-2404.
30. F. Xiong, D. Zhou, Z. Xie and Y. Chen, *Applied Energy*, 2012, 99, 291-296.
31. T. H. Randle and A. T. Kuhn, *J. Chem. Soc., Faraday Trans. 1*, 1983, 79, 1741-1756.
32. E. R. Buyanova, L. G. Matvienko, A. I. Kokorin, G. L. Elizarova, V. N. Parmon and K. I. Zamaraev, *Reaction Kinetics and Catalysis Letters*, 1981, 16, 309-313.
33. K. I. Zamaraev and V. N. Parmon, *Russian Chemical Reviews*, 2007, 52, 817.
34. J. D. Blakemore, N. D. Schley, G. W. Olack, C. D. Incarvito, G. W. Brudvig and R. H. Crabtree, *Chemical Science*, 2010, 2, 94-98.
35. D. Hong, M. Murakami, Y. Yamada and S. Fukuzumi, *Energy and Environmental Science*, 2012, 5, 5708-5716.
36. A. R. Parent, R. H. Crabtree and G. W. Brudvig, *Chemical Society Reviews*, 2013, 42, 2247.
37. A. Paulenova, S. E. Creager, J. D. Navratil and W. Y, *Journal of Power Sources*, 2002, 109, 431-438.
38. *International Pat.,* WO 2013131838, 2013.
39. P. Ge, M. D. Scanlon, P. Peljo, X. Bian, H. Vubrel, A. O'Neill, J. N. Coleman, M. Cantoni, X. Hu, K. Kontturi, B. Liu and H. H. Girault, *Chemical communications (Cambridge, England)*, 2012, 48, 6484.
40. B. Hinnemann, P. G. Moses, J. Bonde, K. P. Jørgensen, J. H. Nielsen, S. Horch, I. Chorkendorff and J. K. Nørskov, *Journal of the American Chemical Society*, 2005, 127, 5308-5309.
41. V. W.-h. Lau, A. F. Masters, A. M. Bond and T. Maschmeyer, *ChemCatChem*, 2011, 3, 1739-1742.
42. W. F. Chen, C. H. Wang, K. Sasaki, N. Marinkovic, W. Xu, J. T. Muckerman, Y. Zhu and R. R. Adzic, *Energy & Environmental Science*, 2013, 6, 943-951.
43. H. Vrubel and X. L. Hu, *Angew. Chem.-Int. Edit.*, 2012, 51, 12703-12706.
44. S. Wirth, F. Harnisch, M. Weinmann and U. Schroeder, *Applied Catalysis B-Environmental*, 2012, 126, 225-230.
45. F. A. Armstrong, *Philos. Trans. R. Soc. B-Biol. Sci.*, 2008, 363, 1263-1270.
46. M. Hara and T. E. Mallouk, *Chemical Communications*, 2000, 1903-1904.
47. L. Ouattara, S. Fierro, O. Frey, M. Koudelka and C. Comninellis, *Journal of Applied Electrochemistry*, 2009, 39, 1361-1367.
48. R. D. L. Smith, M. S. Prévot, R. D. Fagan, Z. Zhang, P. A. Sedach, M. K. J. Siu, S. Trudel and C. P. Berlinguette, *Science*, 2013, 340, 60-63.
49. E. Tsuji, A. Imanishi, K.-i. Fukui and Y. Nakato, *Electrochimica Acta*, 2011, 56, 2009-2016.
50. A. Mills and T. Russell, *Journal of the Chemical Society, Faraday Transactions*, 1991, 87, 1245-1250.

Table of content entry

From junk electricity to hydrogen